ELSEVIER

International Journal of Solids and Structures 41 (2004) 5003–5022

INTERNATIONAL JOURNAL OF SOLIDS and STRUCTURES

www.elsevier.com/locate/ijsolstr

Large-scale testing of 3-D steel frame accounting for local buckling

Seung-Eock Kim *, Kyung-Won Kang

Department of Civil and Environmental Engineering/Construction Tech. Research Institute, Sejong University, Seoul 143-747, South Korea

Received 9 March 2004; received in revised form 9 March 2004
Available online 24 April 2004

Abstract

The ultimate strength testing of space steel frame accounting for local buckling was performed. Considering a majority of large-scale frame tests in the past, only two-dimensional frames or three-dimensional frames comprised of compact section are experimentally studied. Therefore, three-dimensional experiments accounting for local buckling are needed to extend the knowledge of this field. Three two-story, single-bay, and sway allowed frames consisting of non-compact section subjected to proportional vertical and horizontal loads were tested. The details of the test frames, test instruments, and test procedures are presented. The load–displacement curves of the test frames are provided. The experiment results are useful for verification of the three-dimensional analytical models. It was observed that the load carrying capacities calculated by the AISC-LRFD method were 13–21% conservative when compared with those of the experiment. This difference is attributed to the fact that the AISC-LRFD approach does not consider the inelastic moment redistribution but the experiment includes the inelastic redistribution effect.

Keywords: Steel frame test; Stability; Proportional loads; Non-linear analysis; Space steel frame; Local buckling

1. Introduction

The second-order inelastic analysis enables designers to directly evaluate the ultimate strength and behavior of structural system. The direct use of second-order inelastic analysis without member capacity checks is expected to be allowed in future design codes. Over the past 30 years, researchers have developed and validated various methods of performing second-order inelastic analysis on steel frames. Most of these studies can be categorized into one of two types: sophisticated and simplified second-order inelastic analysis. The sophisticated analysis (plastic-zone analysis) uses the highest refinement and is considered accurate (Clarke et al., 1992; Vogel, 1985). However, this analysis is not intended to be used in daily engineering practice, because it is too costly and intensive in computation. The simplified analysis for

* Corresponding author. Tel.: +82-2-3408-3291/3607; fax: +82-2-3408-3332.
E-mail addresses: kiyongan@hotmail.com, sekim@sejong.ac.kr (S.-E. Kim).

0020-7683/$ - see front matter © 2004 Elsevier Ltd. All rights reserved.
doi:10.1016/j.ijsolstr.2004.03.012

practical design uses the concentrated plastic hinge (Kim et al., 2001, 2002, 2003b,c, 2004; Kim and Lee, 2002; Kim and Choi, 2001; Liew et al., 2000; Chen and Kim, 1997). This analysis is verified by calibrating with plastic-zone analysis. The plastic zone analysis also requires an experimental verification in order to confirm its validity, since experimental results provide actual behavior and strength of structures. Therefore, a realistic simulation such as full-scale frame testing is quite necessary.

Two-dimensional two-bay full-size frames were tested by Kanchanalai (1977) to verify the plastic-zone analysis. All frames were bent with respect to the weak axis in order to avoid out-of-plane buckling. Two-dimensional full-size frames were tested by Yarimci (1966) at Lehigh University. The frames were sandwiched and supported laterally by two parallel auxiliary frames preventing out-of-plane buckling. All members were bent in strong axis. A series of four tests was conducted by Avery and Mahendran (2000). Each of the four frames could be classified as a two-dimensional, single-bay, single-story, full-scale sway frame with full lateral restraint and rigid joints. Two-series of tests were conducted by Wakabayashi and Matsui (1972) for a two-dimensional one-story frame and a two-story frame. To prevent out-of-plane buckling, two of the same specimens were set in parallel and connected at the joints and at the mid-length of the members. Harrison (1964) tested the equilateral triangular space frame. A horizontal load (H) was applied on the top of the column and a vertical load of $1.3H$ was applied at mid span of the beam.

Although a number of large-scale frame tests have been conducted in the past 30 years, the majority of those are of only two-dimensional frames. Two-dimensional frames are not a realistic representative model of the behavior of real structures. Recently Kim et al. (2003a) and Kim and Kang (2002) tested two-series of three-dimensional two-story frames subjected to proportional and non-proportional loads. They, however, are comprised of the compact section not being susceptible to local buckling. The aim of this paper is to conduct three-dimensional full-scale frame testing accounting for local buckling.

2. Test frames

Three steel frames were tested. They could be classified as a large scale three-dimensional, two-story, one-bay, rigidly jointed, and sway frame.

2.1. Dimension

The dimensions of all three test frames were identical as 2.5 m wide in X-direction, 3 m long in Y-direction, 1.76 m high from the column-base to the second floor, and 2.2 m high from the second floor to the roof. Fig. 1 shows the dimensions of the test frame. The frames were designed to fail by the combined effects of instability including local buckling and yielding. The dimensions were carefully decided to avoid lateral torsional buckling of a single member. A failure by inelastic lateral torsional buckling of a single member would not be appropriate in investigating global behavior of combined yielding and second-order instability of the frame.

2.2. Three-dimension

Many common steel frame tests in the past were performed with simplified two-dimensional assemblages for ease of testing, even though the real structures were three-dimensional. It is obvious that two-dimensional test has difficulty in simulating three-dimensional behavior including space torsion. Therefore, all three test frames presented in this paper were three-dimensional. A photograph of the test frame is shown in Fig. 2.

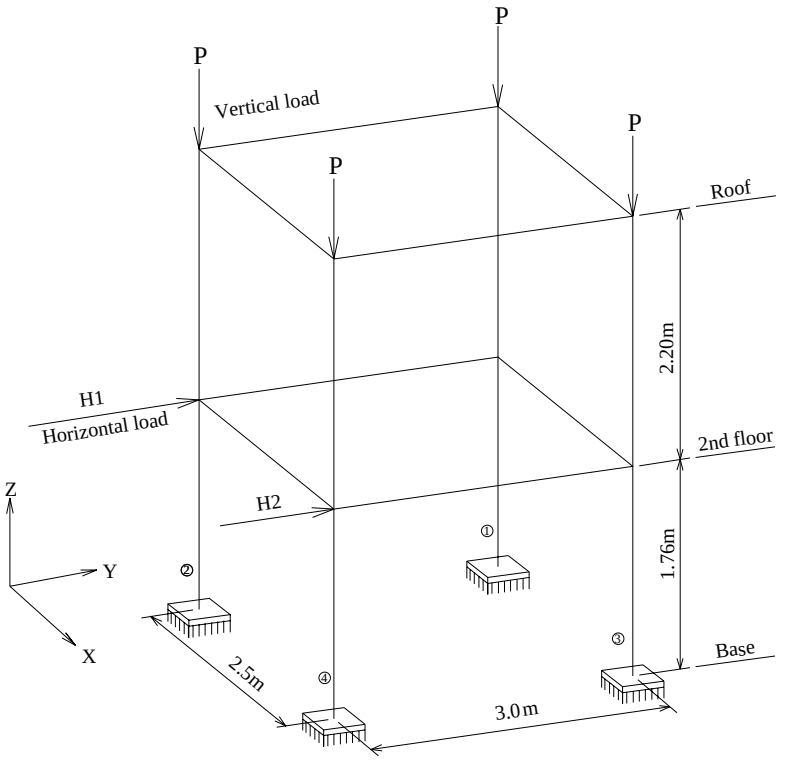

Fig. 1. Dimension and loading condition of test frame.

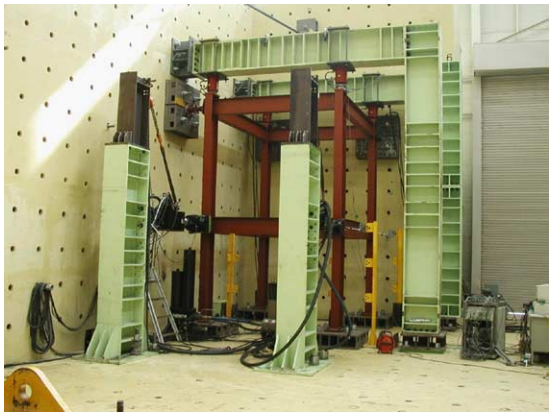

Fig. 2. Test arrangement.

2.3. Sway frame

Sway frames were selected since the stability of sway frames are more complex than that of non-sway frames. The stability of sway frames involves both $P-\Delta$ and $P-\delta$ effects, while that of non-sway frames deals only with $P-\delta$ effects.

2.4. Two-story and single-bay

Previous experimental studies were conducted often for one-story single-bay or sometimes for two-story single-bay frames. Two-story, single-bay frames were chosen in this study. The main reason for selecting two-story frames is that they are convenient in including $P-\Delta$ effect of typical sway frames in the test frames without moving the positions of vertical jacks where the horizontal movements of the test frames at the roof and the second floor level are restrained and free, respectively. Since the same structural principles are used for both two-story, single-bay and more complex multi-story, multi-bay structures, two-story, single-bay frames were enough to investigate structural behavior.

2.5. Structural connection

Structural connections, in general, can be classified as rigid, pinned, or semi-rigid. Rigid connections were used in the test frames. The beam to column connections were fully welded to make rigid connection. Column base connections were made as rigid as possible. The base plate of 40 mm thickness was continuously fillet welded to the column. Each base plate was fastened to the heavily reinforced base block using eight M24 bolts with the center-to-center distance of 200 mm. Fig. 3 shows the connection of the column base.

2.6. Section

Welded wide flange section was used for all three frames. Nominal dimension of the section was H-$300\times150\times3.2\times4.5$ commonly used in Korea. The dimensions and properties of the section are listed in Table 1. The section is non-compact so that it is susceptible to local buckling.

2.7. Material

Material used was grade SS400 steel with nominal yield stress of 250 MPa, commonly used in Korea.

Fig. 3. Column ② base connection and strain gauge.

Table 1
Dimensions and properties of section H-300×150×3.2×4.5 used in the frame

Nos. 1–3	Height H (mm)	Width B (mm)	Thickness of flange t_f (mm)	Thickness of web t_w (mm)	Radius of fillet r_1 (mm)	Gross area A_g (mm^2)	Moment of inertia about X axis I_X (10^6 mm^4)	Moment of inertia about Y axis I_Y (10^6 mm^4)
Nominal	300	150	4.50	3.20	–	2281	36.04	2.53
Measured								
Column	300	150	4.47	3.40	–	2332	36.27	2.51
Beam	300	150	4.43	3.46	–	2337	36.16	2.49

3. Test instrument

3.1. General

The frames were tested in the strong floor, wall, and loading frame which could sustain 2000 kN. The strong floor and wall were 1.0 and 2.0 m thick, respectively. The photograph of the test setup is shown in Fig. 2.

3.2. Loading frame

The height from the strong floor surface to the top of the loading frame was 5.45 m and the distance from the shear wall surface to the inner face of the loading frame column was 4.4 m. The column base of the loading frame was fastened with 16 M24 bolts to the heavily reinforced base block, which was fastened again with four M50 bolts to the strong floor. The one end of the girder of the loading frame was fastened with 16 M24 bolts to the base block, which was bolted again with four M50 bolts to the strong wall. The other end of the girder was fastened with 16 M24 bolts to the column. The girder and column depth and width of the loading frame were 0.6 and 0.4 m, respectively. The flange and web thickness were 25 and 19 mm, respectively.

3.3. Hydraulic jack

Four 1000 kN hydraulic jacks with 100 mm stroke were mounted at the bottom flange of the loading frame girder in alignment with the center of each of the four columns of the test specimens so that the vertical loads could be applied to the columns without eccentricity. The four vertical jacks were connected by one pump so that they could produce equal loads simultaneously. A 1000 kN load cell was installed under the hydraulic jack and on the top of the column ④. A single load cell was enough to measure the applied loads, since the hydraulic jacks generated equal loads. Fig. 4 shows the four vertical jacks and the load cell.

Forty millimeter thick steel plate was welded to transfer the vertical jack forces to the flange and web of the columns ①, ②, and ③ preventing local crushing of the column web. A thinner plate of 20 mm was used for the column ④ since the load cell diameter placed on the top of the column ④ was 150 mm which was bigger than the piston diameter of 125 mm of the hydraulic jack.

Fig. 4. Four vertical jacks and one load cell.

3.4. Actuator

Two actuators were installed on the flanges of the two loading columns at the height of 2.03 m from the strong floor surface. The sectional dimensions of the loading columns were identical with those of the loading frame members. The base of the loading columns was fastened with six M50 bolts to the strong floor. The actuators generated horizontal loads applied at the second floor level of the test frame.

3.5. Boundary condition of test frame

The test frame was semi-fixed in displacement and rotation at the base level, free to move at the second floor level, and fixed in displacement at the roof level. The base plates of the four columns of the test frame were fastened with eight M24 bolts to the heavily reinforced base block, which was fastened again with four M50 bolts to the strong floor. The horizontal displacements of the test specimen at the roof level were restrained by the three screw-jack supports. The restraint was provided so that the vertical jack force was applied on the top of the column, since it was difficult to move the jacks horizontally as the test specimen deformed. Although the test frame is different from the actual sway frame, it contains $P-\Delta$ effect which is a key factor of a typical sway frame. The main reason for selecting two-story frame is its convenience in including $P-\Delta$ effect. Fig. 5 shows the screw-jack support.

A small convex shape plate was welded to the front face of the screw-jack in order to simulate the ideal roller support under the vertical loads.

3.6. Instrument of measurement

The actuators would measure the horizontal displacements caused not only at the test frame but also at the loading column at the second floor level. Linear variable differential transformers (LVDTs) were installed to measure the real horizontal displacement at the columns ② and ④ of the test frame. Fig. 6 shows the actuator and the corresponding LVDT. Figs. 7 and 8 show the corresponding LVDTs, respectively. LVDT was installed to check the horizontal slip of the base plate as shown in Fig. 4. The electric signals from the five LVDTs, two actuators, and one load cell were fed directly into a data acquisition system which was connected again to the computer system, closely monitoring the behavior of the test frame during the test.

Fig. 5. Screw-jack support.

Fig. 6. Horizontal actuator and LVDT at second floor level.

Fig. 7. LVDT (column ②).

Fig. 8. LVDT (column ③).

4. Test procedure and results

4.1. Material test

Stress–strain curves were obtained by tensile testing. The tensile testing was conducted in accordance with the Korean standard KS B 0801. The measured dimensions of the beam members were different from those of the column members as listed in Table 1, although the nominal dimensions of the beam and column members were identical as H-300×150×3.2×4.5. Six specimens were tested. Each specimen was taken from the flange and web of the test frames, respectively. The stress–strain data obtained from the tensile testing of the specimen is shown in Table 2. The strain hardening started at the strain range from 0.025 to 0.039. The unloading occurred at the strain range of 0.17–0.23. The specimens had higher yield stresses ranging from 370 to 396 MPa than the nominal yield stress of 250 MPa. The ultimate stress of the specimens was approximately 450 MPa which was within the range of the nominal stress of 400–510 MPa.

4.2. Pre-Test

Although the column base was intended to be rigidly connected, the rigidly bolted connection cannot be achieved in real situation. The Pre-Test was conducted to evaluate the flexibility of the bolted connection of the column base. For the Pre-Test, no restraint was provided at the roof level in order to make boundary condition as simple as possible. Two actuators applied identical horizontal loads on columns ② and ④ of the test frame.

The horizontal load was increased up to 60 kN so that the test frame will remain within an elastic range. The LVDT measured the horizontal displacements at the columns ② and ④ at the second floor level. The load–displacement relationship is listed in Table 3. The horizontal displacement was used to determine the connection flexibility at the column base.

4.3. Measure of imperfections

The out-of-plumbness of the columns in X and Y directions was measured using an electro-optical system. The out-of-straightness was not measured since it did not make significant difference on the

Table 2
Multi-linear stress–strain curves for H-300×150×3.2×4.5 steel

No. 1	Flange	Stress (MPa)	0	374	374	411	440	448	445	435	407
		Strain	0	0.00185	0.02500	0.04787	0.09993	0.17126	0.22459	0.26364	0.30634
	Web	Stress (MPa)	0	396	396	430	454	459	457	450	428
		Strain	0	0.00196	0.02879	0.05759	0.11276	0.16808	0.20917	0.24747	0.28557
No. 2	Flange	Stress (MPa)	0	371	371	420	441	446	442	430	401
		Strain	0	0.00186	0.02360	0.05886	0.10931	0.16953	0.23364	0.27530	0.31392
	Web	Stress (MPa)	0	398	398	436	460	464	461	455	439
		Strain	0	0.00196	0.02462	0.05912	0.11661	0.17304	0.21667	0.25611	0.29360
No. 3	Flange	Stress (MPa)	0	368	368	390	416	438	441	438	428
		Strain	0	0.00182	0.02626	0.03661	0.06268	0.11994	0.16919	0.22643	0.26995
	Web	Stress (MPa)	0	393	393	424	450	456	454	446	419
		Strain	0	0.00196	0.03986	0.05675	0.11229	0.17434	0.21755	0.25763	0.30070

Table 3
Horizontal displacement of test frame by Pre-Test

Test frame	Displacement of the column ②	Displacement of the column ④
No. 1	4.702	4.701
No. 2	4.575	4.529
No. 3	4.617	4.614

Table 4
Measured out-of-plumbness imperfections

Test frame	Level	Imperfections (mm)							
		Column ①		Column ②		Column ③		Column ④	
		X	*Y*	*X*	*Y*	*X*	*Y*	*X*	*Y*
No. 1	Roof	−3.04	−6.81	−1.29	−4.49	1.43	4.16	−9.51	−6.17
	Second floor	7.74	−4.28	1.89	−3.64	4.94	6.04	−2.07	−3.57
	Base	0	0	0	0	0	0	0	0
No. 2	Roof	−3.61	−5.03	2.82	−1.44	0.52	5.42	−0.43	0.89
	Second floor	−1.98	−4.43	0.53	−0.23	2.54	5.89	−0.65	−0.16
	Base	0	0	0	0	0	0	0	0
No. 3	Roof	1.50	−9.49	−11.81	−7.22	−8.17	11.53	4.02	6.27
	Second floor	0	−4.68	−2.47	−3.04	−0.53	7.61	1.30	1.62
	Base	0	0	0	0	0	0	0	0

behavior of unbraced frames. The measured out-of-plumbness was summarized in Table 4. A positive imperfection indicates that the column was offset in the positive direction in the X and Y axes in Fig. 1.

Table 5
Load case of test frame

Test frame	Vertical load	Horizontal load (H_1)	Horizontal load (H_2)
No. 1	P	$P/3$	$P/6$
No. 2	P	$P/4$	$P/8$
No. 3	P	$P/5$	$P/10$

4.4. Main test

Vertical and horizontal loads increased at the same time. The vertical loads were applied on the top of the four columns, and the horizontal loads were applied on the columns ② and ④ at the second floor level of the test frame. The load cases of the three test frames are listed in Table 5.

The test stopped when column ② could not sustain any more load. The horizontal loads were automatically increased according to the specified load ratio for each test frame controlled by the computer system. After the onset of nonlinear load–displacement relationship of each test frame, the loading rate was reduced. The time required to finish each test was approximately 30 min. The frame failed by instability including local buckling and yielding. The buckled shape at the column ② of test frame is shown in Figs. 9–11. Five strain gauges were attached to the column ② as shown in Fig. 12. The horizontal load–strain (in vertical direction) curves are illustrated in Figs. 13–15. The strain increased dramatically just after local buckling occurred. The LVDT measured the horizontal displacements of the columns ②, ③, and ④ at the second floor level. The arrangement of LVDTs is shown in Fig. 16. The load–displacement curves are shown in Figs. 17–19. The curves can be used to verify numerical analysis results. The load carrying capacities of each test frame are listed in Table 6. The load carrying capacities indicate the maximum load that the test frame can sustain.

5. Numerical analysis

The obtained results from 3-D non-linear analysis were compared with experimental data. ABAQUS, one of mostly widely used and accepted commercial finite element analysis program, was used (Kim and Lee, 2002). ABAQUS S4R and STRI35 shell element were used for the analyses of test frame (Fig. 20).

Fig. 9. Local buckling of the column ② at the base level (test frame no. 1).

Fig. 10. Local buckling of the column ② at the base level (test frame no. 2).

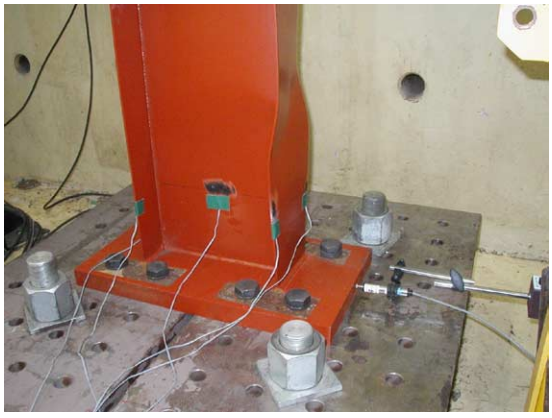

Fig. 11. Local buckling of the column ② at the base level (test frame no. 3).

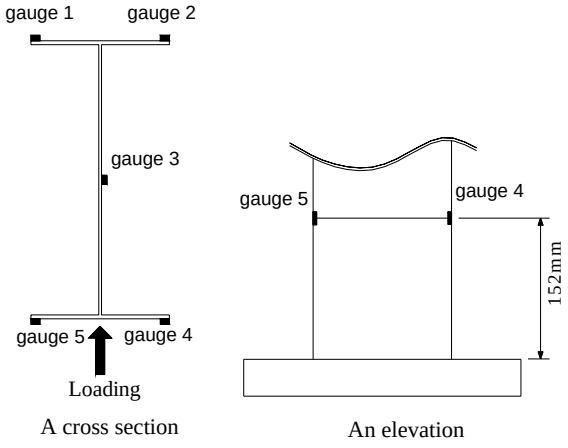

Fig. 12. Strain gauge.

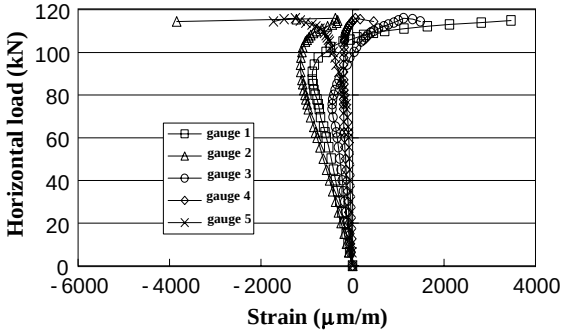

Fig. 13. Stress–strain curve (test frame no. 1).

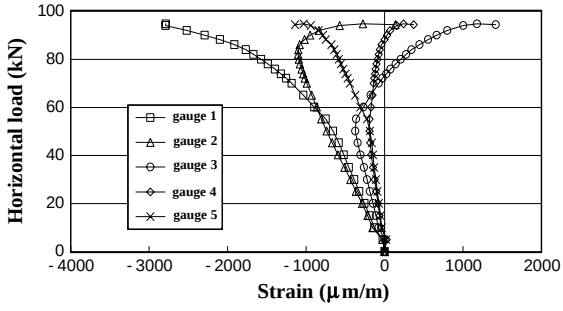

Fig. 14. Stress–strain curve (test frame no. 2).

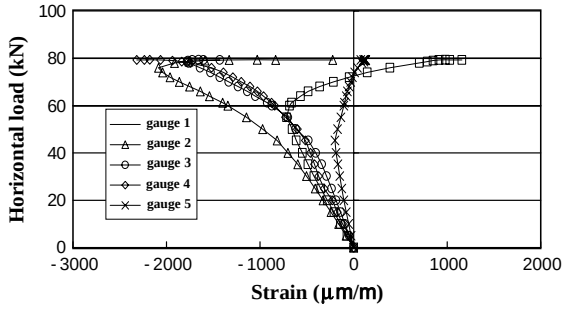

Fig. 15. Stress–strain curve (test frame no. 3).

Sixteen elements through the depth of the web and eight elements across the width of the flange were used (Fig. 21). An aspect ratio close to unity was used in the direction of flange width and web depth. The base plate connection was simulated by horizontal and vertical springs used at each nodal point. The spring constants were varied in the numerical model of Pre-Test frame until the analytical and experimental results agreed. The horizontal and vertical spring constants attached at 41 nodes of the base plate were determined

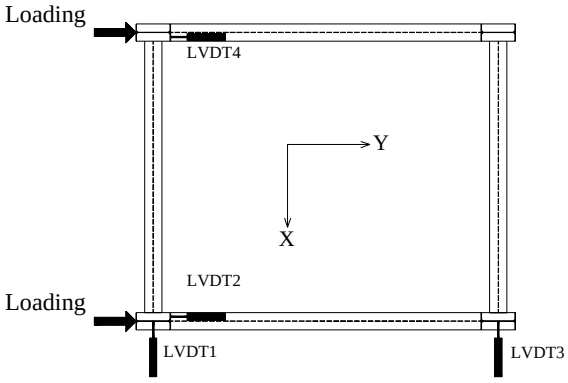

Fig. 16. Arrangement of LVDT.

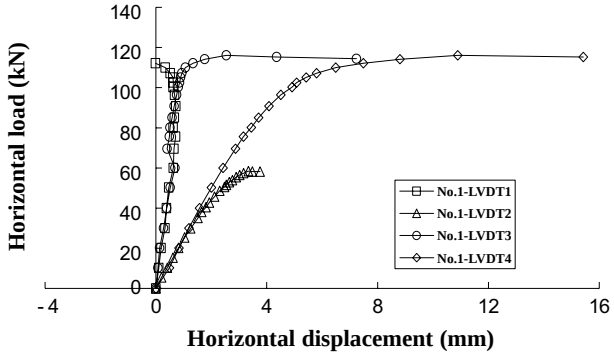

Fig. 17. Horizontal load–displacement curve for test frame (test frame no. 1).

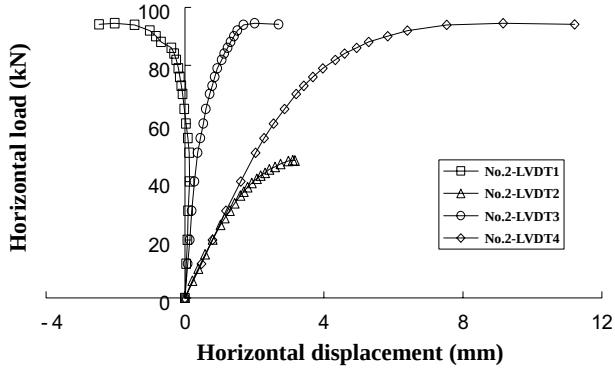

Fig. 18. Horizontal load–displacement curve for test frame (test frame no. 2).

as 61,846 KN/m. The horizontal and vertical spring constants were assumed identical due to limited data obtained by Pre-Test. The multi-linear stress–strain curves listed in Table 2 were used. The nominal

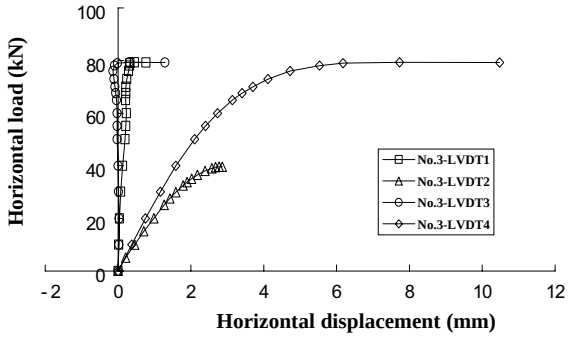

Fig. 19. Horizontal load–displacement curve for test frame (test frame no. 3).

Table 6
Comparison of experimental, analysis, and design load carrying capacities

Test fame		(a) Experiment	(b) Analysis	(c) AISC-LRFD design	(b)/(a)	(c)/(a)
No. 1	P	313.80	339.66	249.65	1.0824	0.7956
	H_1	104.45	113.22	83.22	1.0840	0.7967
	H_2	52.56	56.61	41.61	1.0771	0.7917
No. 2	P	339.20	363.6	285.02	1.0719	0.8403
	H_1	85.05	90.9	71.26	1.0688	0.8379
	H_2	42.65	45.45	35.63	1.0657	0.8354
No. 3	P	356.00	364.5	311.41	1.0239	0.8747
	H_1	71.46	72.9	62.28	1.0201	0.8715
	H_2	35.74	36.45	31.14	1.0199	0.8713

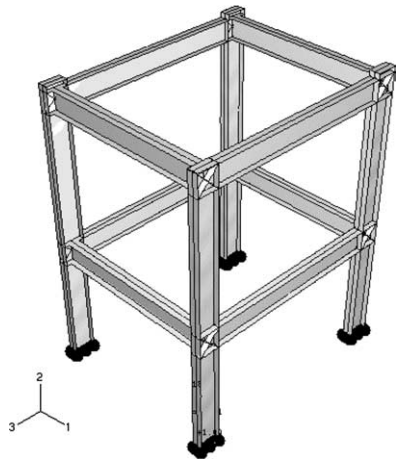

Fig. 20. 3-D finite element modeling.

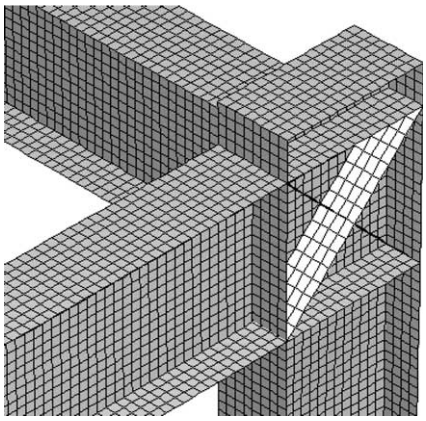

Fig. 21. Finite element mesh.

Table 7
Yield stress and elastic modulus

Test fame		Yield stress (MPa)	Elastic modulus (MPa)
No. 1	Flange	374	202,293
	Web	396	201,856
No. 2	Flange	371	199,399
	Web	398	202,643
No. 3	Flange	368	201,739
	Web	393	200,678

stress–strain data obtained by a uniaxial test are available they may be simply converted to the true stress and logarithmic plastic strain as

$$\sigma_{\text{true}} = \sigma_{\text{nom}}(1 + \varepsilon_{\text{nom}}), \qquad \varepsilon_{\text{ln}}^{\text{pl}} = \ln(1 + \varepsilon_{\text{nom}}) - \frac{\sigma_{\text{true}}}{E}$$

where σ_{true}, σ_{nom}, $\varepsilon_{\text{ln}}^{\text{pl}}$, ε_{nom}, and E are true stress, nominal stress, logarithmic plastic strain, nominal strain, and Young's modulus, respectively. The measured elastic moduli and yield stresses listed in Table 7 were used. Poisson's ratio used was 0.3.

The magnitude of the measured imperfections in the test frames was listed in Table 4. Out-of-plumbness imperfections, however, were not explicitly modeled since the magnitude was not significant. Out-of-straightness imperfections were not included since $P - \delta$ effects in unbraced frames are not dominant. Local imperfections were modeled since the test frame was comprised of non-compact sections. Imperfection shape was determined by performing 40 eigenvalue analyses. Eight eigenmodes were combined to simulate local imperfection. The maximum magnitude of the local imperfections used is shown in Fig. 22. The longitudinal membrane residual stress distributions recommended by ECCS Technical Committee 8 (ECCS, 1984) was adopted (Fig. 23). The maximum residual stress was selected as 100% of the yield stress. The residual stress distributions were modeled using ABAQUS *INITIAL CONDITIONS option. The initial stresses were defined using the SIGINI FORTRAN user subroutine. These subroutines define the local components of the initial stress as a function of the element number.

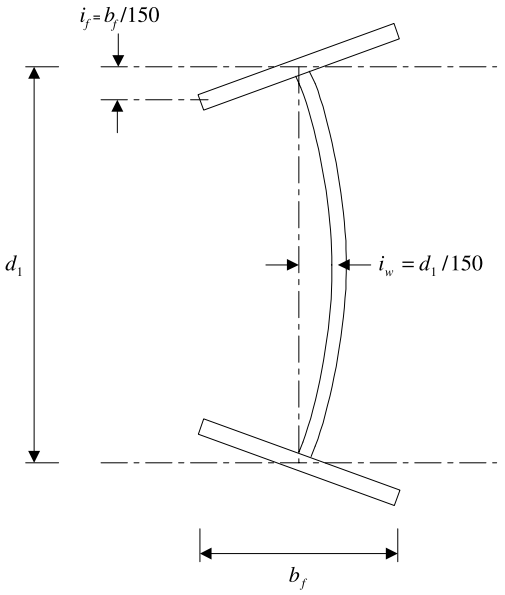

Fig. 22. Local imperfections.

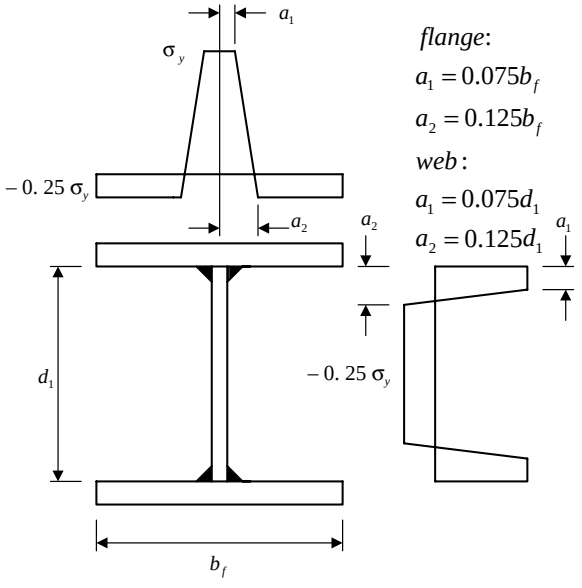

Fig. 23. Assumed residual stress distribution for welded I-sections.

The vertical concentrated nodal forces representing the vertical jack loads were applied at the top of each column without eccentricity. A horizontal concentrated nodal forces representing the horizontal jack loads were applied concentrically to the outside flange of the columns ② and ④ at the second floor level (Fig. 1). Geometric and material non-linear static analysis was used to obtain the ultimate load carrying capacity.

The arc-length method with the minimum time increment of 10^{-5} s was used for non-linear analyses. The analysis terminated automatically when numerical instability occurred.

Deflected shape at ultimate state is shown in Fig. 24. Local buckling at the base level of the column ② is shown in Fig. 25. The horizontal load–deflection curves obtained from the analysis are compared with the experimental curves in Figs. 26–28. The ultimate load obtained from non-linear analysis and the experiment data are nearly same, within 2–8.4% difference as listed in Table 6. The horizontal displacements obtained

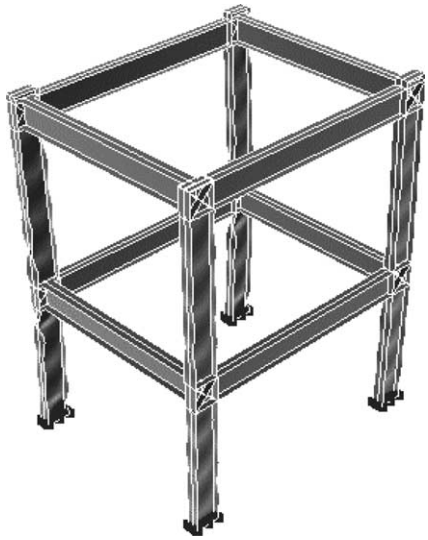

Fig. 24. Deflected shape of test frame at ultimate state.

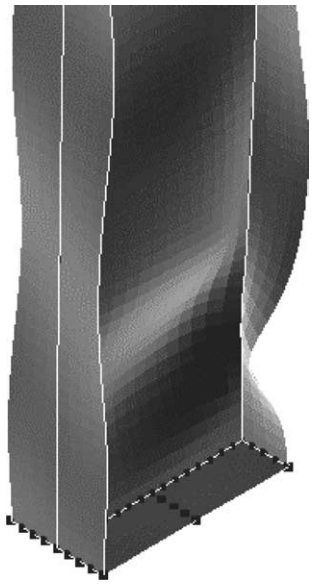

Fig. 25. Local buckling at the base level of the column ②.

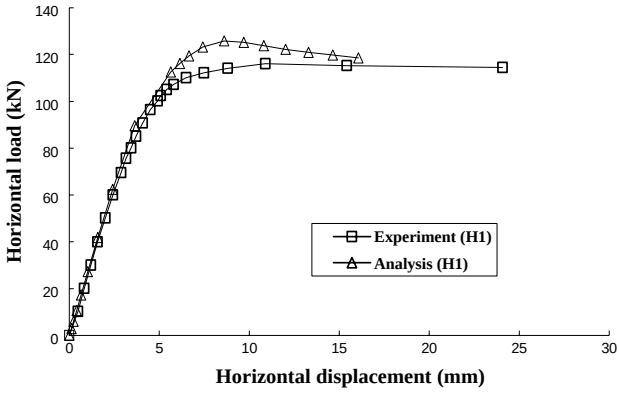

Fig. 26. Compare experiment with analysis (test frame no. 1).

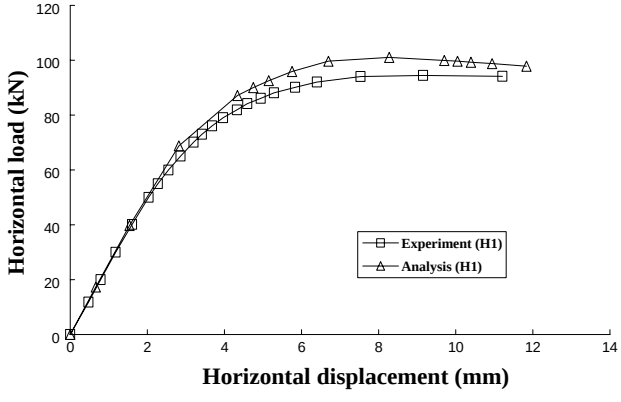

Fig. 27. Compare experiment with analysis (test frame no. 2).

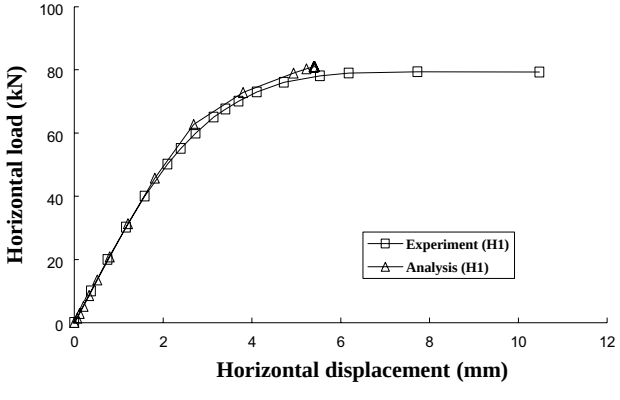

Fig. 28. Compare experiment with analysis (test frame no. 3).

from the experiment and the analysis show some difference. This difference can be attributed to possible experimental errors (i.e., boundary conditions, eccentric loading, variations in the material properties, and

residual stresses) and analytical approximations (i.e., nominal residual stresses, imperfection distributions, and simplified stress–strain curves).

6. Comparison of test results with AISC-LRFD capacities

Load carrying capacities obtained by the experiment, 3-D analysis, and AISC-LRFD method are compared in Table 5. The AISC-LRFD capacities were obtained using the average measured yield stresses of the flange and web specimens. A resistance factor of 0.9 was used in the experiment and analysis capacity, while factors of 0.85 for columns and 0.9 for beams were used in the AISC-LRFD capacity. The results showed that the AISC-LRFD capacities were approximately 13–21% conservative. This difference is derived from the fact that the AISC-LRFD approach does not consider the inelastic moment redistribution, but the experiment and analysis include the inelastic redistribution effect. This comparison provides concrete reasons to use an inelastic nonlinear analysis which is quite necessary to reduce member sizes. It is important to note that the conventional design approach using semi-empirical specification equations for separate member capacity checks after linear elastic analysis of a structures system should be replaced by advanced analysis (inelastic nonlinear analysis) in a near future.

7. Conclusions

Large-scale testing of 3-D steel frame accounting for local buckling is summarized and concluded as follows:

(1) Considering the majority of large-scale frame tests in the past, only two-dimensional frames or three-dimensional frames comprised of compact section are experimentally studied. Therefore, this three-dimensional experiment accounting for local buckling can be regarded quite valuable.
(2) The three test frames are a large-scale three-dimensional, two-story, one-bay, rigidly jointed, and sway frame, subjected to proportional vertical and horizontal loads. The test frames were carefully designed to fail by local buckling.
(3) Although the column base was intended to be rigidly connected, the rigidly bolted connection cannot be achieved in real situation. The Pre-Test was conducted to evaluate the flexibility of the bolted connection of the column base. The spring constants were varied in the numerical model of Pre-Test frame until the analytical and experimental results agreed. The horizontal and vertical spring constants attached at 41 nodes of the base plate were determined as 61,846 KN/m. The horizontal and vertical spring constants were assumed identical due to limited data obtained by Pre-Test.
(4) The load–displacement curves of the test frames are provided. The experiment results are useful for verification of three-dimensional analytical models. The ultimate load obtained from the experiment and non-linear analysis is agreed well within 2–8.4% difference. The horizontal displacement between the experiment and the analysis shows some difference. This is attributed to possible experimental errors and analytical approximations.
(5) The experiment results showed that the load carrying capacities calculated by the AISC-LRFD method was 13–21% conservative compared with the experimental results. This difference is derived from the fact that the AISC-LRFD approach does not consider the inelastic moment redistribution but the experiment includes the inelastic redistribution effect. It is important to note that the conventional design approach using semi-empirical specification equations for separate member capacity checks after linear elastic analysis of a structures system should be replaced by advanced analysis (inelastic nonlinear analysis) in a near future.

Acknowledgements

This work presented in this paper was supported by funds of National Research Laboratory Program (Grant No. 2000-N-NL-01-C-162) from Ministry of Science and Technology in Korea. Authors wish to appreciate the financial support.

References

Avery, P., Mahendran, M., 2000. Large-scale testing of steel frame structures comprising non-compact sections. Eng. Struct. 22, 920–936.

Chen, W.F., Kim, S.E., 1997. LRFD Steel Design Using Advanced Analysis. CRC Press, Boca Raton, FL.

Clarke, M.J., Bridge, R.Q., Hancock, G.J., Trahair, N.S., 1992. Benchmarking and verification of second-order elastic and inelastic frame analysis programs. In: White, D.W., Chen, W.F. (Eds.), SSRC TG 29 Workshop and Monograph on Plastic Hinge Based Methods for Advanced Analysis and Design of Steel Frames, SSRC, Lehigh University, Bethlehem, PA.

ECCS, 1984. Ultimate limit state calculation of away frames with rigid joints. Technical Committee 8-Structural Stability Technical Working Group 8.2-System, Publication No. 33, European Convention for Constructional Steelwork.

Harrison, H.B., 1964. The Application of the principles of plastic analysis to three-dimensional steel structures. Ph.D. Thesis, Department of Civil Engineering, University of Sydney.

Kanchanalai, T., 1977. The design and behavior of beam-columns in unbraced steel frames. AISI Project No. 189, Report No. 2, Civil Engineering/Structures Research Lab., University of Texas at Austin, 300 pp.

Kim, S.E., Choi, S.H., 2001. Practical advanced analysis for semi-rigid space frames. Solid Struct. 38, 9111–9131.

Kim, S.E., Kang, K.W., 2002. Large-scale testing of space steel frame subjected to non-proportional loads. Solid Struct. 39 (26), 6411–6427.

Kim, S.E., Lee, D.H., 2002. Second-order distributed plasticity analysis of space steel frames. Eng. Struct. 24, 735–744.

Kim, S.E., Park, M.H., Choi, S.H., 2001. Direct design of three-dimensional frames using practical advanced analysis. Eng. Struct. 23, 1491–1502.

Kim, S.E., Lee, J.H., Park, J.S., 2002. 3-D second-order plastic-hinge analysis accounting for lateral torsional buckling. Solid Struct. 39, 2109–2128.

Kim, S.E., Kang, K.W., Lee, D.H., 2003a. Full-scale testing of space steel frame subjected to proportional loads. Eng. Struct. 25 (1), 69–79.

Kim, S.E., Choi, S.H., Ma, S.S., 2003b. Performance based design of steel arch bridges using practical inelastic nonlinear analysis. J. Construct. Steel Res. 59, 91–108.

Kim, S.E., Lee, J.H., Park, J.S., 2003c. 3-D second-order plastic-hinge analysis accounting for local buckling. Eng. Struct. 25 (1), 81–90.

Kim, S.E., Lee, J.S., Choi, S.H., Kim, C.S., 2004. Practical second-order inelastic analysis for steel frames subjected to distributed load. Eng. Struct. 26, 51–61.

Liew, R.J.Y., Chen, H., Shanmugam, N.E., Chen, W.F., 2000. Improved nonlinear plastic hinge analysis of space frame structures. Eng. Struct. 22, 1324–1338.

Vogel, U., 1985. Calibrating frames. Stahlbau. 10, 1–7.

Wakabayashi, M., Matsui, C., 1972. Elastic–plastic behaviors of full size steel frame. Trans. Arch. Inst. Jpn. 198, 7–17.

Yarimci, E., 1966. Incremental inelastic analysis of framed structures and some experimental verification. Ph.D. Dissertation, Department of Civil Engineering, Lehigh University, Bethlehem, PA.